

**Secular Trends in Global Tides derived from Satellite Radar Altimetry**

I. Bij de Vaate<sup>1</sup>, D. C. Slobbe<sup>1</sup>, M. Verlaan<sup>2,3</sup>

<sup>1</sup>Civil Engineering and Geosciences, Delft University of Technology, Delft, The Netherlands

<sup>2</sup>Delft Institute of Applied Mathematics, Delft University of Technology, Delft, The Netherlands

<sup>3</sup>Deltares, Delft, Netherlands

**Contents of this file**

Text S1 and S2.  
Figures S1 to S7

**Introduction**

This supporting information describes the analysis that was performed to assess the sensitivity of estimated  $S_2$  amplitudes to the ionospheric altimetry correction (Text S1) and the method to compare secular trends at TPJ-crossovers with trends derived from tide gauges (Text S2 & Figure S1). In addition, it contains figures (S2-S3) depicting the 95% confidence intervals of the trend estimates based on the confidence intervals of the tidal harmonic constants, as computed by UTide and based on the model approach. Thereafter, Figure S4 and S5 show the co-phase lines derived from satellite altimetry at the start and end of the TPJ-period. Finally, the linear changes derived from the SegHA approach (see 3.1 Segmented Harmonic Analysis (SegHA)) are incorporated in Figure S6 (global) and Figure S7 (North West European Shelf).

**Text S1** Sensitivity analysis of estimated  $S_2$  tidal harmonic constants to ionospheric altimeter correction

One of the geophysical corrections that is applied to the TPJ altimetry data is the ionospheric correction. This can be either an altimeter-derived correction or a modeled correction (NIC09 for TOPEX/Poseidon and GIM for Jason1-3) (Scharroo et al., 2016). As demonstrated by Zawadzki et al. (2018), any error in these corrections would cause a signal at the alias frequency of  $S_2$ . In addition, they showed that replacing the altimeter-derived correction by the modeled correction alters the amplitude of the  $S_2$  signal by up to 3 mm.

To assess the sensitivity of the analysis described in the paper to the choice of ionospheric correction, an additional experiment was carried out. For this purpose, the TPJ data of ~500 random crossovers across the globe was corrected by the model-derived ionospheric correction and the radar-derived correction respectively. Consequently, the data were processed and analyzed as described in the paper (following both the SegHA and TintHA approach). The resulting linear change in  $S_2$  amplitudes were compared by computing the mean absolute differences. Note that crossovers close to land or sea ice were ignored, because the radar-derived ionospheric correction is likely deteriorated there (Fernandes et al., 2014).

It was found that the impact of the ionospheric correction was largest near the equator (mean differences of 0.15 mm/year) and reduced at higher latitudes ( $< 0.05$  mm/year). This is in line with Figure 7 from Zawadzki et al. (2018). The differences were subsequently interpolated to all crossover locations, multiplied by 1.96 and added to the confidence intervals of the  $S_2$  amplitudes that were computed by UTide (Figure S2a) and the model-based alternative (Figure S3a). To get an idea of the impact of this additional "ionospheric error", one could compare Figure S2a and 4a). As the initial confidence intervals outputted by UTide are the same for all semi-diurnal tides (e.g.  $S_2$  and  $M_2$ ), the difference between Figure S2a and 4a is solely due to the ionospheric error.

**Text S2** Quantification of agreement between secular trends derived from tide gauges and at TPJ-crossovers.

The following method has been implemented to compare the degree of similarity between secular trends in tidal amplitude derived at TPJ-crossovers and from tide gauge (TG) records (from the GESLA-3 dataset; Haigh et al., 2021). First, the complete TG data within the domain with more than 18 years of data during the TPJ-period (1432 locations) were used to quantify the spatial variability in the trends as a function of distance between two locations (spVAR; see Figure S1a). This has been done using the median absolute deviation. As can be seen in Figure S1b, the distance between tide gauges and TPJ-crossovers with sufficient data varies between ~50 km and > 400 km. For the comparison, only TGs were considered that are closer than 75 km to one or more TPJ-crossovers. This leaves 195 TGs (locations can be found in Figure 5 and 6).

Subsequently, for all TG-crossover combinations, the absolute differences in estimated trend were computed. Finally, the agreement was classified as being *good (medium, low)* for TG-crossover combinations where the difference in estimated trends is less than 1 time (2 times, 3 times) the standard error (SE) of the trend estimate at the crossover (as derived from the model approach, see Figure S3) plus the spVAR. *No agreement* was assigned to remaining TG-crossover combinations (Figure S1c). Values mentioned in the paper correspond to *good + medium* agreement.

Note that such a comparison between secular trends derived at TPJ-crossover locations and from tide gauge records should be treated with caution because of numerous reasons (see paper).

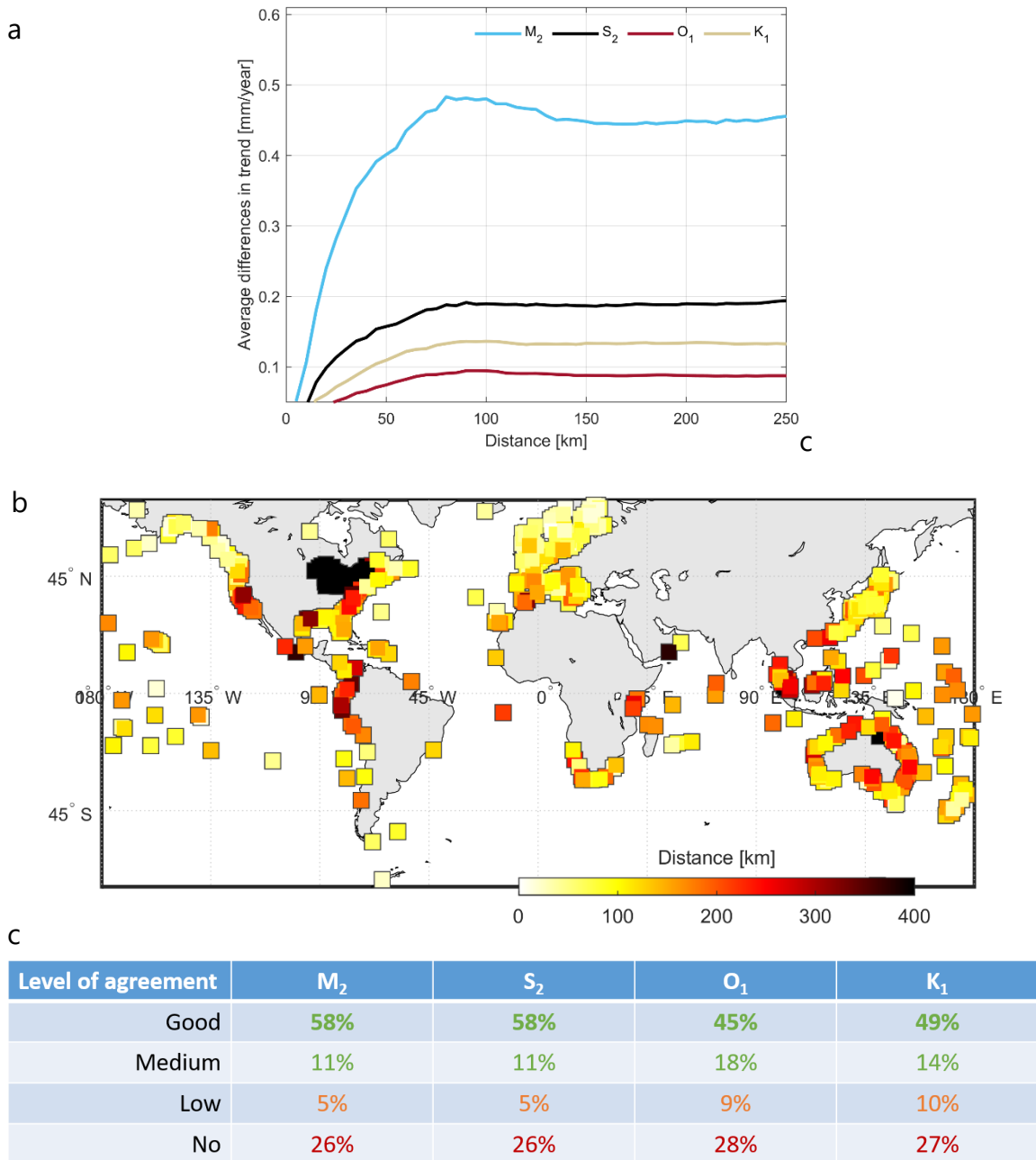


**Figure S1.** Spatial variability in estimated secular trends in tidal amplitude (median absolute deviation) derived from tide gauge data (a). Distance between each tide gauge and the nearest TPJ-crossover (b). The percentages of TG-crossover combinations that show *good*, *medium*, *low* or *no agreement* with nearby tide gauges are displayed in (c) for the four considered tides (TintHA approach).

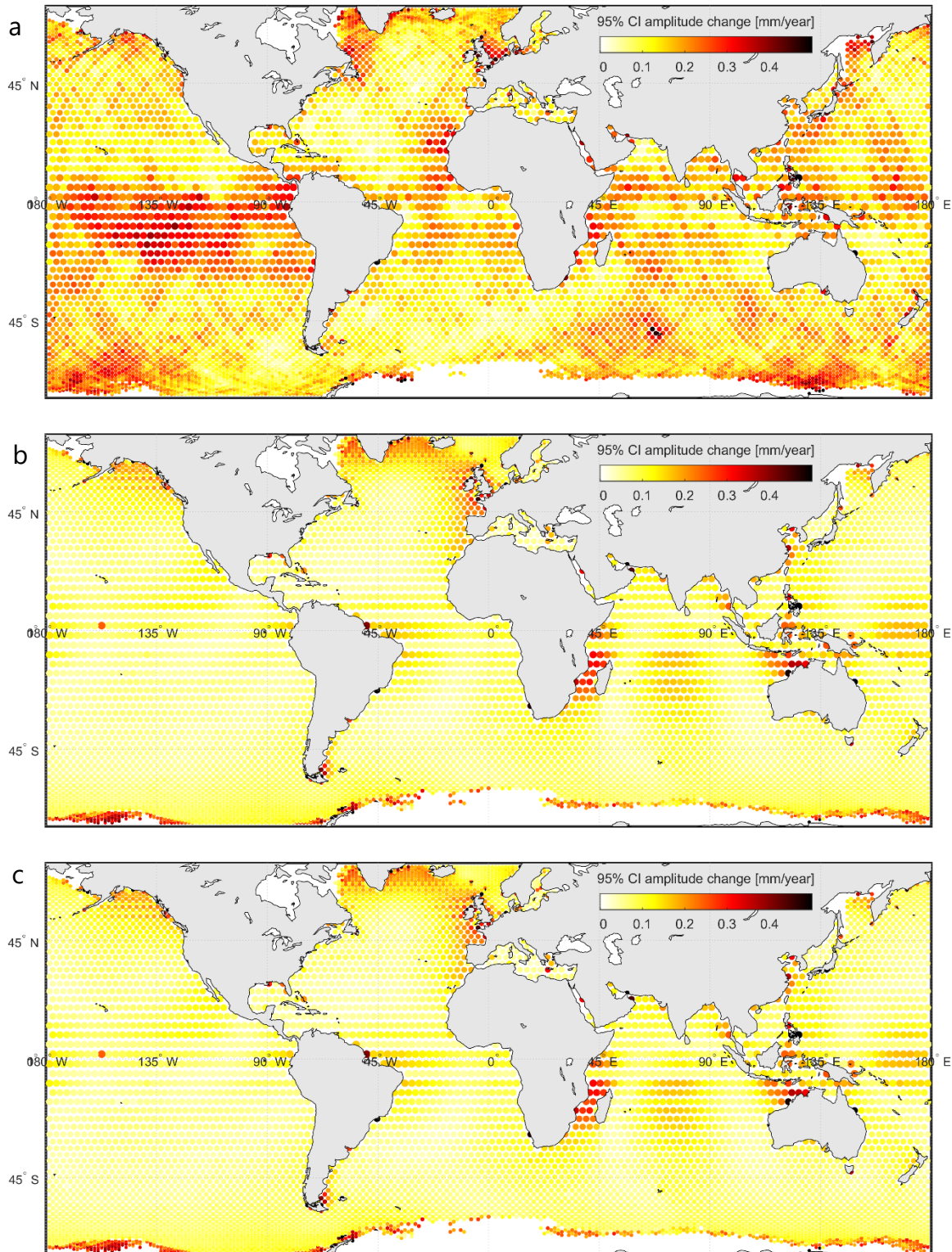


**Figure S2.** 95% confidence intervals for trend estimates derived from amplitude standard errors computed by UTide following the TinTHA approach, for  $S_2$  (a),  $O_1$  (b) and  $K_1$  (c). The intervals for  $S_2$  include the sensitivity to the ionospheric correction as explained in Text S1.

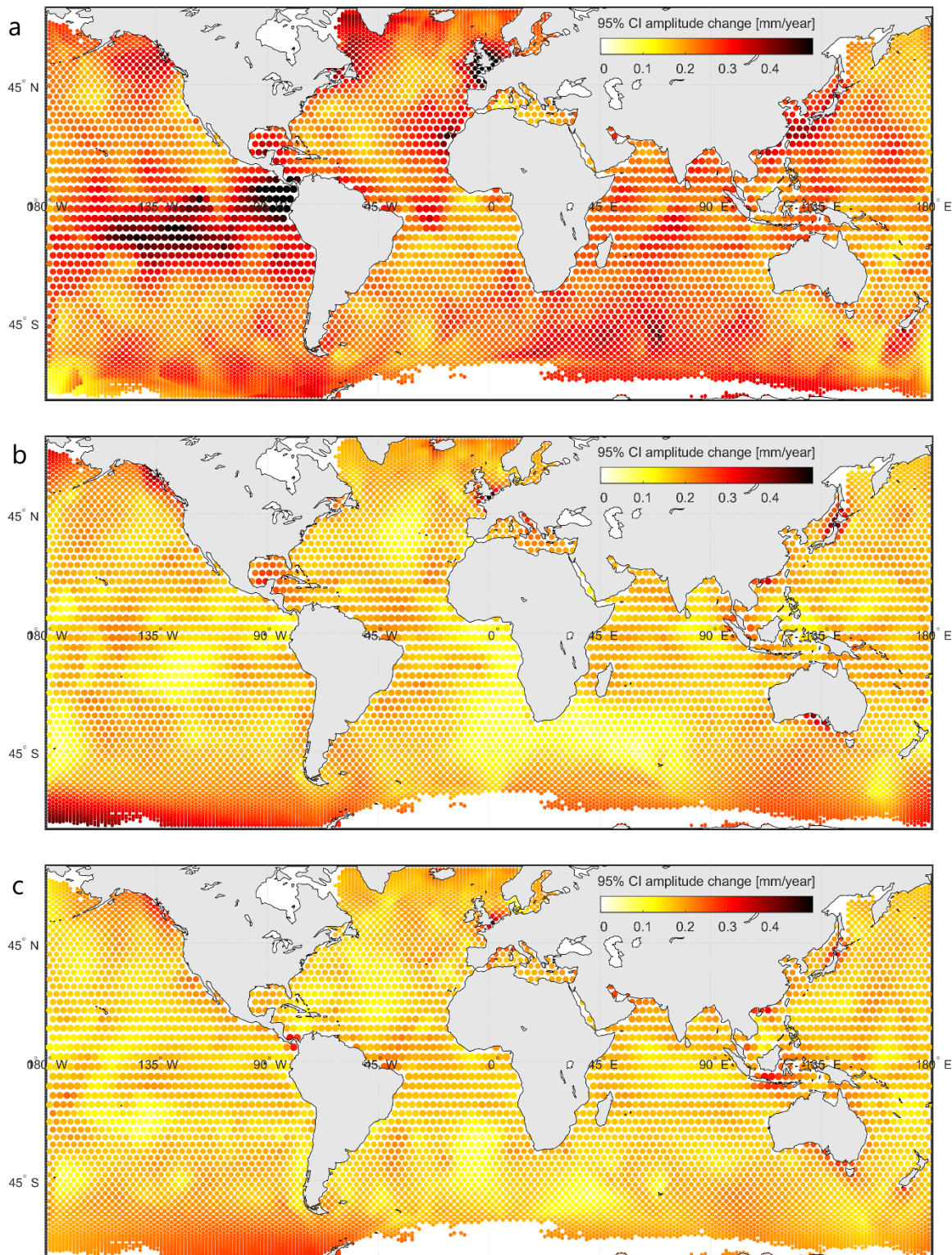


**Figure S3.** 95% confidence intervals for trend estimates derived from amplitude standard errors derived from model approach described in paper following the TintHA approach, for  $S_2$  (a),  $O_1$  (b) and  $K_1$  (c). The intervals for  $S_2$  include the sensitivity to the ionospheric correction as explained in Text S1.

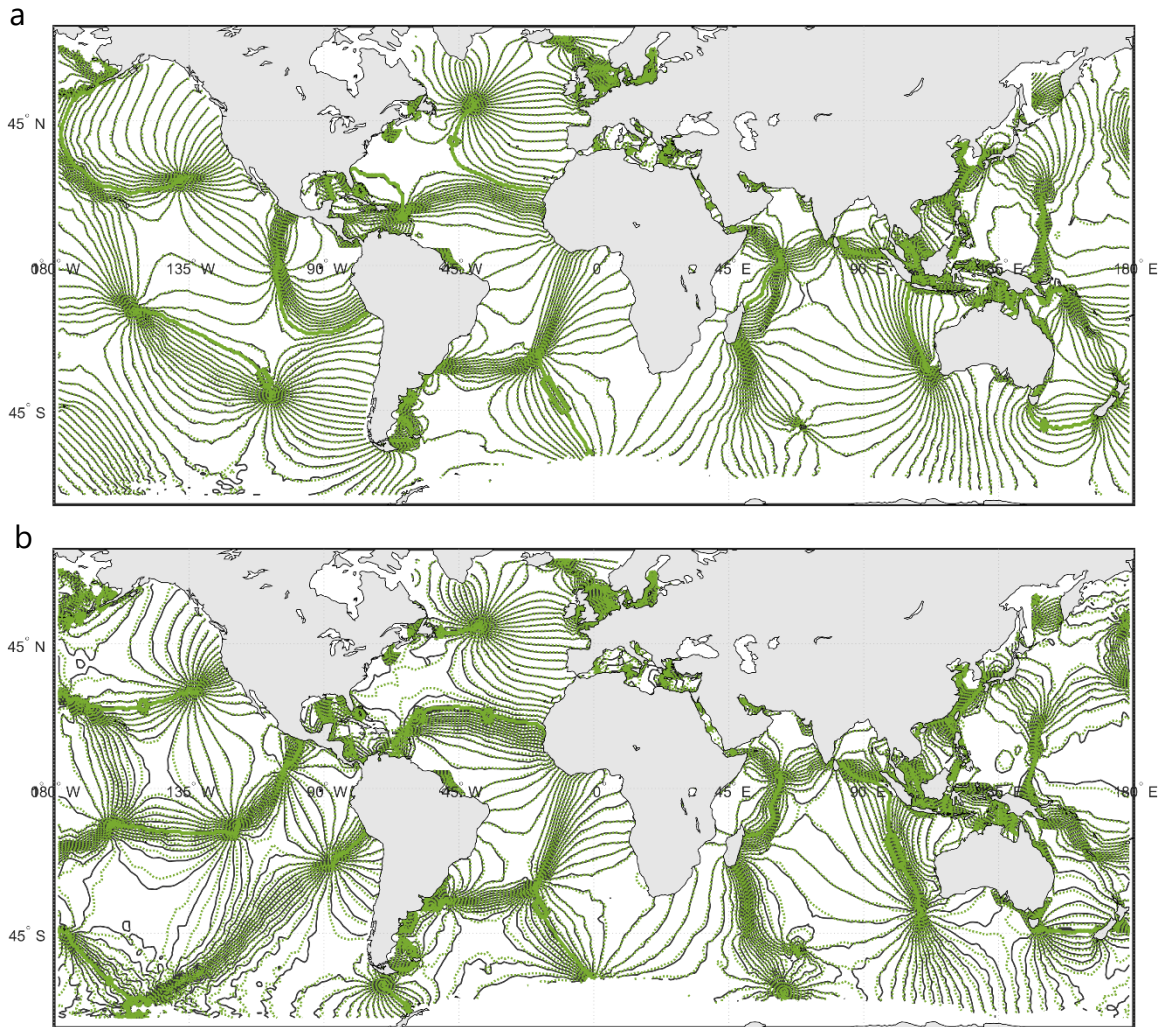


**Figure S4.** Cotidal phase lines at 10-degree intervals, for 1993 in black and for 2020 in green: M<sub>2</sub> (a), S<sub>2</sub> (b), derived by TinTHA approach.

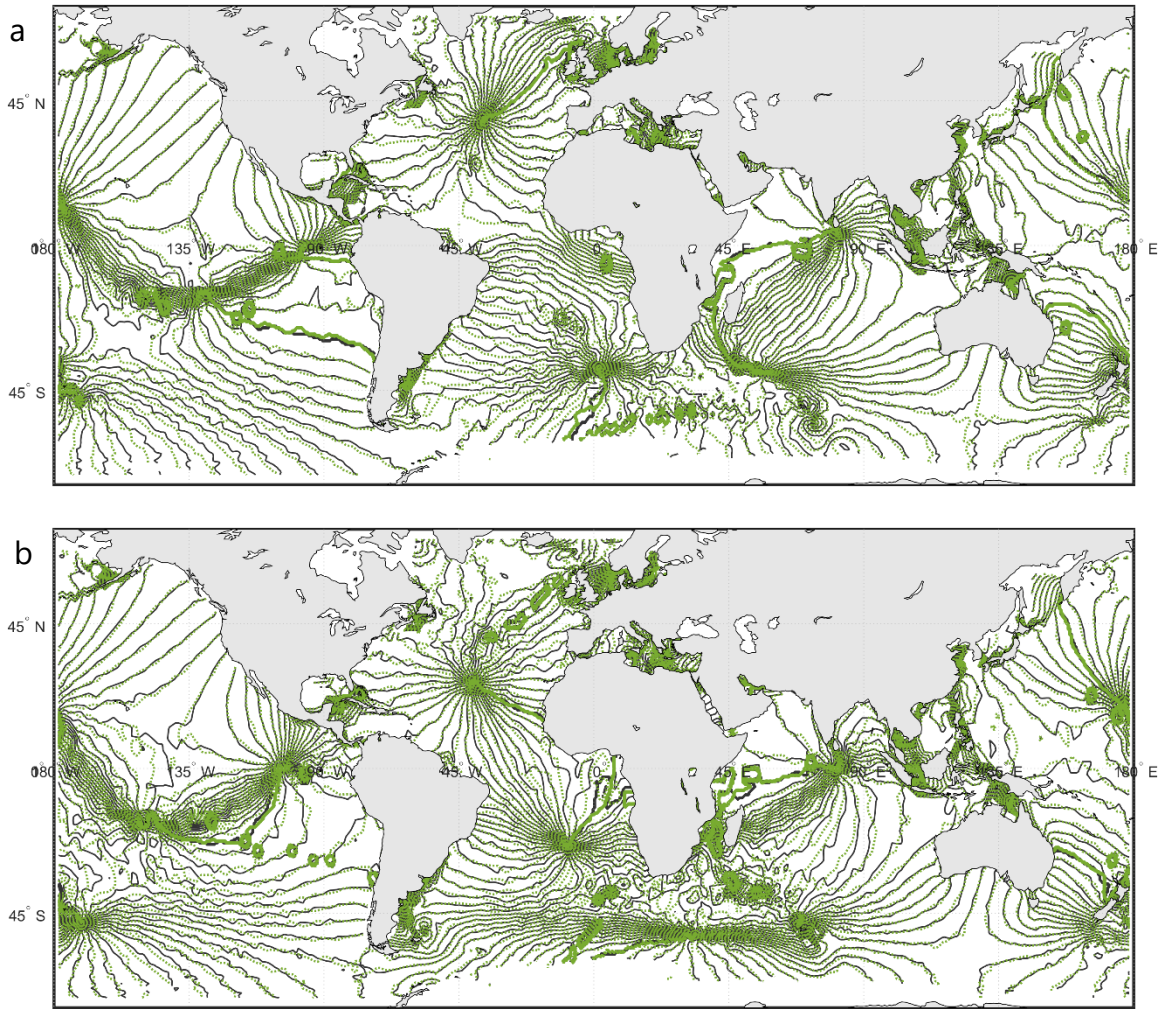


**Figure S5.** Cotidal phase lines at 10-degree intervals, for 1993 in black and for 2020 in green:  $O_1$  (a),  $K_1$  (b), derived by T-IN HA approach.

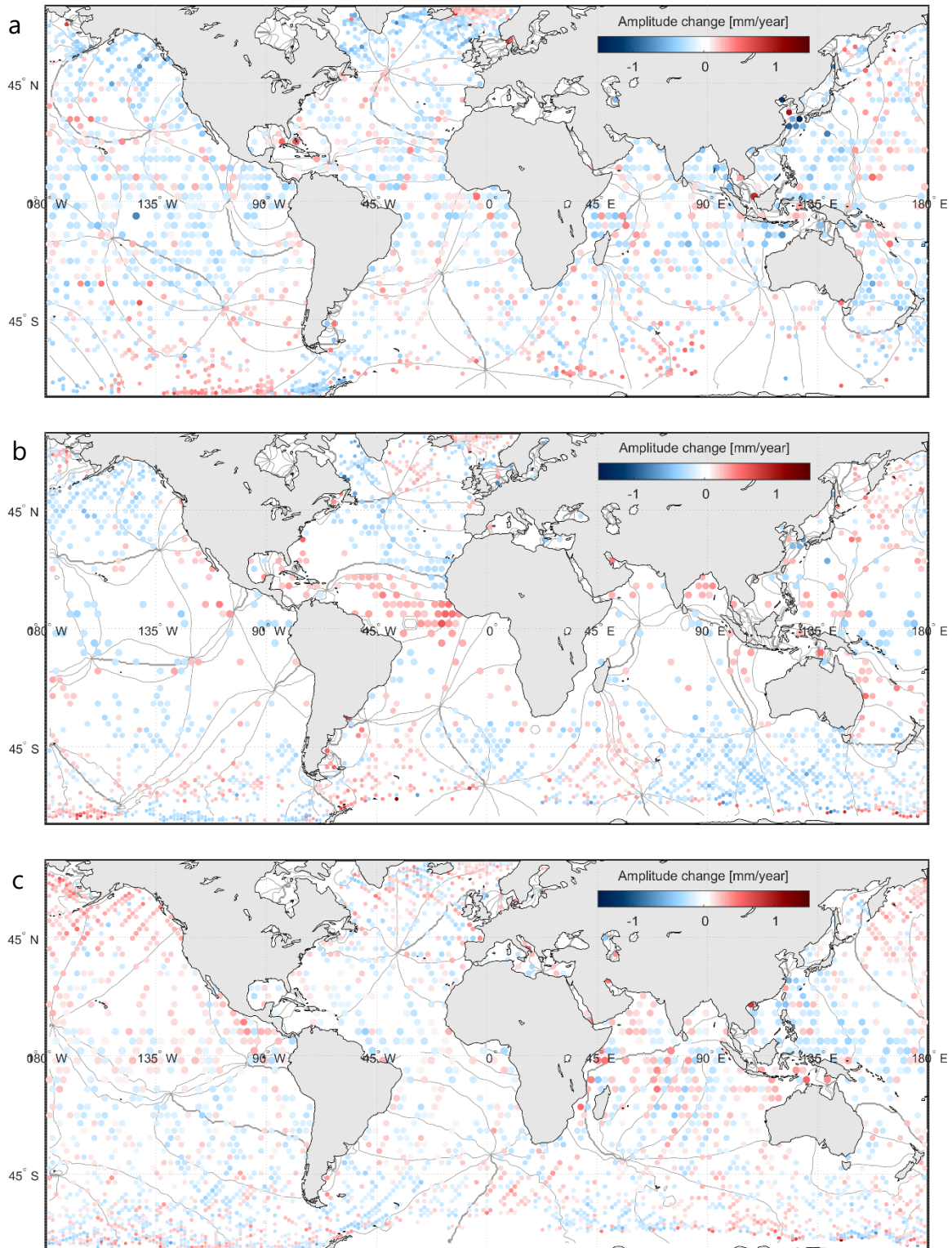


**Figure S6.** Linear change in  $M_2$  amplitude (a),  $S_2$  (b), and  $O_1$  (c) per year (1993-2020) following from the SegHA approach. Scatter size reduces with latitude to reduce cluttering at high latitudes. Locations where the post-processing criteria (including both data- and model-based 95% confidence intervals) were not met are excluded from the figure. Lines in the background depict tidal phases at  $45^\circ$  intervals.

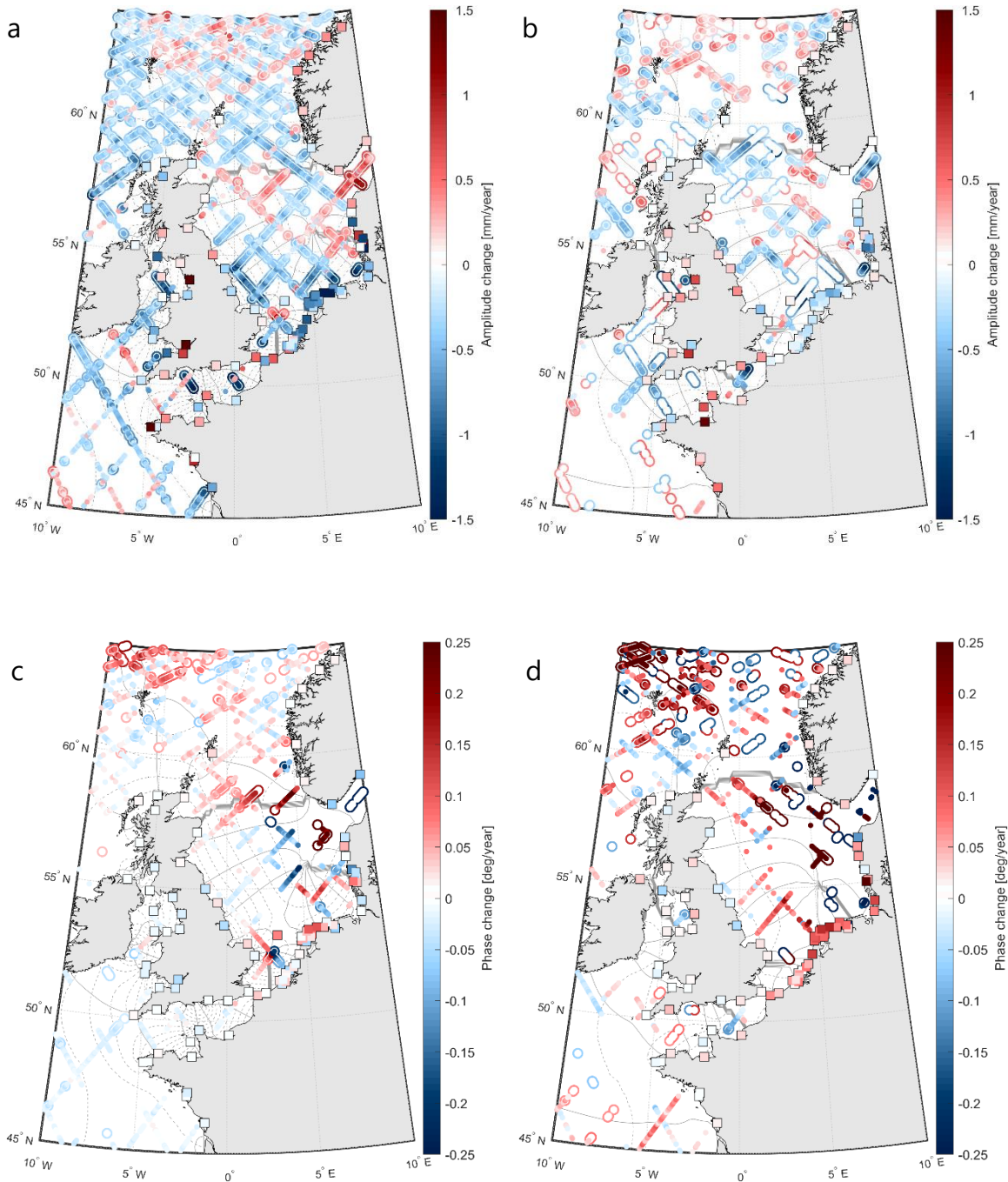


**Figure S7.** Linear change in M<sub>2</sub> amplitude (a), S<sub>2</sub> amplitude (b), M<sub>2</sub> phase (c) and S<sub>2</sub> phase (d) per year derived by the SegHA approach. The smaller solid scatters indicate significant trends given the data-based confidence intervals, the hollow outline indicates significance according to the model-based confidence intervals as described in the paper. Co-tidal maps are shown in the background where the solid line indicates the phase at 45° intervals, the dashed lines show the amplitudes at 0.25 m intervals.